

On Memorization in Probabilistic Deep Generative Models

Gerrit J.J. van den Burg¹
gertjanvandenburgh@gmail.com

Christopher K.I. Williams^{2,1}
ckiwi@inf.ed.ac.uk

¹ The Alan Turing Institute, London, UK

² The University of Edinburgh, Edinburgh, UK

June 8, 2021

Abstract

Recent advances in deep generative models have led to impressive results in a variety of application domains. Motivated by the possibility that deep learning models might memorize part of the input data, there have been increased efforts to understand how memorization can occur. In this work, we extend a recently proposed measure of memorization for supervised learning (Feldman, 2019) to the unsupervised density estimation problem and simplify the accompanying estimator. Next, we present an exploratory study that demonstrates how memorization can arise in probabilistic deep generative models, such as variational autoencoders. This reveals that the form of memorization to which these models are susceptible differs fundamentally from mode collapse and overfitting. Finally, we discuss several strategies that can be used to limit memorization in practice.

Keywords: Memorization, Generative Models, Density Estimation, Unsupervised Learning

1 Introduction

In the last few years there have been incredible successes in generative modeling through the development of deep learning techniques such as variational autoencoders (VAEs) [1, 2], generative adversarial networks (GANs) [3], normalizing flows [4, 5], and diffusion networks [6], among others. The goal of generative modeling is to learn the data distribution of a given data set, which has numerous applications such as creating realistic synthetic data, correcting data corruption, and detecting anomalies. Novel architectures for generative modeling are typically evaluated on how well a complex, high dimensional data distribution can be learned by the model and how realistic the samples from the model are. An important question in the evaluation of generative models is to what extent observations from the training data are *memorized* by the learning algorithm.

A common technique to assess memorization in deep generative models is to look for nearest neighbors. Typically, several samples are drawn from a trained model and compared to their nearest neighbors in the training set. There are several problems with this approach. First, it has been well established that when using the Euclidean metric this test can be easily fooled by taking an image from the training set and shifting it by a few pixels [7]. For this reason, nearest neighbors in the feature space of a secondary model are sometimes used, as well as cropping and/or downsampling before identifying nearest neighbors (e.g. [8–10]). Second, while there may not be any neighbors in the training set for a small selection of samples from the model, this does not demonstrate that there are *no* observations that are highly memorized. Indeed, in several recent publications on deep generative models it is possible to identify some observations highly similar to the training set in the illustrations of generated samples (see Supplement A).

Memorization in generative models is not always surprising. When the training data set contains a number of highly similar observations, such as duplicates, then it would be expected that these receive an increased weight in the model and are more likely to be generated. The fact that commonly-used data sets contain numerous (near) duplicates [11] therefore provides one reason for memorization of training observations. While important, memorization due to duplicates is not the focus of this work. Instead, we are concerned with memorization that arises as *an increased probability of generating a sample that closely resembles the training data in regions of the input space where the algorithm has not seen sufficient observations to enable generalization*. For example, we may expect that highly memorized observations

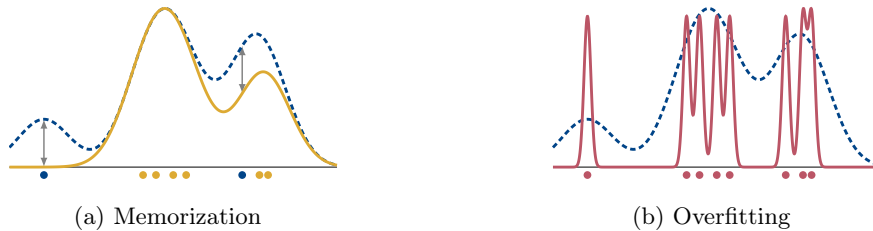


Figure 1: Memorization vs. overfitting. In (a) the dashed blue curve reflects the probability density when all observations are included, whereas the solid yellow curve is the density when only yellow observations are included. The local change in density that occurs when an observation is removed from the training data indicates the extent to which the model memorized the observation. The density typically associated with overfitting due to overtraining is shown by the solid red curve in (b).

are either in some way atypical or are essential for properly modeling a particular region of the data manifold.

Figure 1a illustrates this kind of local memorization in probabilistic generative models. In certain regions of the input space the learned probability density can be entirely supported by a single, potentially outlying, observation. When sampling from the model in these parts of the space it is thus highly likely that a sample similar to an input observation will be generated. The figure also illustrates that in regions of the input space that are densely supported by closely-related observations, sampling will yield observations that resemble the input data. The change in the probability density of an observation that occurs when it is removed from the data forms the basis of the memorization score we propose in Section 3. This form of memorization should be contrasted with what is commonly associated with memorization due to overfitting (illustrated in Figure 1b), which generally occurs when a model is trained for too long or with too high a learning rate (*overtraining*). Hence, we observe that in generative models memorization and generalization can occur simultaneously at distinct regions of the input space, and are not necessarily caused by overtraining.

To understand memorization further, consider the simple case of fitting a single multivariate normal distribution to a data set. In this scenario, the presence or absence of a particular observation in the data set will have a small effect on the learned model unless the observation is an outlier. By contrast, a kernel density estimate (KDE) [12, 13] of the probability density may be more sensitive to the presence or absence of a particular observation. To see why this is the case, consider that in sparsely-populated regions of the input space the KDE can be supported by a relatively small number of observations. Although deep generative models typically operate in much higher dimensional spaces than the aforementioned methods, the same problem can arise when generalizing to regions of the space that are weakly supported by the available data. Because these models are optimized globally, the model has to place some probability mass in these regions. As we will demonstrate below, it is not necessarily the case that the model places low probability on these observations, resulting in observations that are both highly memorized when present in the data set, but also not significantly less likely under the model than other observations.

In this work, we extend a recently proposed measure of memorization for supervised learning [14, 15] to probabilistic generative models and introduce a practical estimator of this memorization score. We subsequently investigate memorization experimentally, where we focus on the variational autoencoder. In our experiments we demonstrate that highly memorized observations are not necessarily outliers, that memorization starts to occur early during the training process, and show the connection between nearest neighbor tests for memorization and the proposed memorization score. Finally, we discuss several approaches that can limit memorization in practice.

2 Related Work

Here we review related work on memorization in deep learning models, memorization as it relates to membership inference, the evaluation of generative models, and influence functions.

Memorization in deep learning. The observation that deep learning models can learn from patterns of random data has been a catalyst for recent efforts to understand memorization in supervised learning [16–18]. A number of approaches have been proposed to test for memorization in specific applications. In [19] memorization in language models is evaluated using a “canary” string (e.g. if “my social security

number is x ” is in the training data, how often does the model complete the prompt using x instead of a comparable $y \neq x$ that is not in the training set). Unfortunately, this approach does not translate easily to other contexts, such as images. Moreover, language models often contain explicit memory cells that can facilitate memorization, which are absent in most generative models.

A memorization score for supervised learning was proposed in [14, 15], which forms the inspiration for our formulation in Section 3. A related “consistency score” for supervised learning was proposed in [20]. We argue, however, that memorization in supervised learning differs fundamentally from that in generative models, as the label prediction task affects the training dynamics, and label noise is known to induce memorization in supervised learning [21, 22]. Building on earlier work by [23, 24], a hypothesis test is proposed in [25] that is based on the premise that memorization has occurred when samples from the trained model are “closer” to the training data than observations from the test set. While this is a useful test for aggregate memorization behavior in (a region of) the input space, our proposed score function allows us to quantify the memorization of a single observation.

Membership inference. A topic closely related to memorization is the problem of membership inference. Here, the goal is to recover whether a particular observation was part of the unknown training data set, either using knowledge of the model, access to the model, or in a black-box setting. Membership inference is particularly important when models are deployed [26], as potentially private data could be exposed. In the supervised learning setting, [27] propose to use an attack model that learns to classify whether a given sample was in the training set. Later work [28, 29] focused on generative models and proposed to train a GAN on samples from the target model. The associated discriminator is subsequently used to classify membership of the unknown training set. A related approach to recovering training images is described in [30], using an optimization algorithm that identifies for every observation the closest sample that can be generated by the network. However this requires solving a highly non-convex problem, which isn’t guaranteed to find the optimal solution.

Evaluating generative models. Memorization is a known issue when evaluating generative models, in particular for GANs [24, 31]. Several approaches are discussed in [7], with a focus on the pitfalls of relying on log-likelihood, sample quality, and nearest neighbors. Using the log-likelihood can be particularly problematic as it has been shown that models can assign higher likelihood to observations outside the input domain [32]. Nowadays, generative models are frequently evaluated by the quality of their samples as evaluated by other models, as is done in the Inception Score (IS) [33] and Fréchet Inception Distance (FID) [34]. Since these metrics have no concept of where the samples originate, the pathological case where a model memorizes the entire training data set will yield a near-perfect score. Motivated by this observation, [35] propose to use neural network divergences to measure sample diversity and quality simultaneously, but this requires training a separate evaluation model and there is no guarantee that *local* memorization will be detected.

Influence functions. The problem of memorization is also related to the concept of *influence functions* in statistics [36, 37]. Influence functions can be used to measure the effect of upweighting or perturbing an observation. Recently, influence functions have been considered as a diagnostic tool for deep learning [38, 39]. However, it has also been demonstrated that influence function estimates in deep learning models can be fragile [40]. Below, we therefore focus on a relatively simple estimator to gain a reliable understanding of memorization in probabilistic deep generative models.

3 Memorization Score

We present a principled formulation of a memorization score for probabilistic generative models, inspired by the one proposed recently in [14, 15] for supervised learning. Let \mathcal{A} denote a randomized learning algorithm, and let a be an instance of the algorithm (i.e., a trained model). Here, \mathcal{A} captures a complete description of the algorithm, including the chosen hyperparameters, training epochs, and optimization method. The randomness in \mathcal{A} arises from the particular initial conditions, the selection of mini batches during training, as well as other factors. Denote the training data set by $\mathcal{D} = \{\mathbf{x}_i\}_{i=1}^n$ with observations from $\mathcal{X} \subseteq \mathbb{R}^D$. Let $[n] = \{1, \dots, n\}$ and write $\mathcal{D}_{\mathcal{I}} = \{\mathbf{x}_i : \mathbf{x}_i \in \mathcal{D}, i \in \mathcal{I}\}$ for the subset of observations in the training data indexed by the set $\mathcal{I} \subseteq [n]$. The posterior probability assigned to an observation $\mathbf{x} \in \mathcal{X}$ by a model a when trained on a data set \mathcal{D} is written as $p(\mathbf{x} | \mathcal{D}, a)$.

Algorithm 1 Computing the Cross-Validated Memorization Score

Input: Algorithm \mathcal{A} , data set \mathcal{D} , repetitions t , folds K

Output: $\hat{M}(\mathcal{A}, \mathcal{D}, i)$, $\forall i$

```
1: for  $\ell = 1, \dots, t$  do
2:    $\mathcal{G}_\ell \leftarrow$  Random partition of  $[n]$  into  $K$  disjoint subsets
3:   for  $\mathcal{I}_{\ell,k} \in \mathcal{G}_\ell$  with  $k = 1, \dots, K$  do
4:      $a_{\ell,k} \leftarrow$  Train  $\mathcal{A}$  on  $\mathcal{D}_{[n] \setminus \mathcal{I}_{\ell,k}}$ 
5:      $\pi_{\ell,k,i} \leftarrow$  Compute  $\log p(\mathbf{x}_i \mid \mathcal{D}_{[n] \setminus \mathcal{I}_{\ell,k}}, a_{\ell,k})$ ,  $\forall i \in [n]$ 
6:   end for
7: end for  $\triangleright \text{LOGMEANEXP}(\{\mathbf{u}_i\}_{i=1}^n) = -\log n + \text{LOGSUMEXP}(\{\mathbf{u}_i\}_{i=1}^n)$ 
8:  $U_i \leftarrow \text{LOGMEANEXP}(\{\pi_{\ell,k,i} : \ell \in [t], k \in [K], i \notin \mathcal{I}_{\ell,k}\})$ ,  $\forall i$ 
9:  $V_i \leftarrow \text{LOGMEANEXP}(\{\pi_{\ell,k,i} : \ell \in [t], k \in [K], i \in \mathcal{I}_{\ell,k}\})$ ,  $\forall i$ 
10:  $\hat{M}(\mathcal{A}, \mathcal{D}, i) \leftarrow U_i - V_i$ ,  $\forall i$ 
```

We are interested in the posterior probability of an observation assigned by the algorithm \mathcal{A} , not merely by an instantiation of the algorithm. Therefore we introduce the probability $P_{\mathcal{A}}(\mathbf{x} \mid \mathcal{D})$ and its sampling estimate as

$$P_{\mathcal{A}}(\mathbf{x} \mid \mathcal{D}) = \int p(\mathbf{x} \mid \mathcal{D}, a) p(a) da \approx \frac{1}{T} \sum_{\ell=1}^T p(\mathbf{x} \mid \mathcal{D}, a_\ell), \quad (1)$$

for some number of repetitions T . We see that $P_{\mathcal{A}}(\mathbf{x} \mid \mathcal{D})$ is the expectation of $p(\mathbf{x} \mid \mathcal{D}, a)$ over instances of the randomized algorithm \mathcal{A} .

To facilitate meaningful interpretation of the memorization score we use the difference in log probabilities, in contrast to [14, 15]. Thus we define the memorization score as

$$M(\mathcal{A}, \mathcal{D}, i) = \log P_{\mathcal{A}}(\mathbf{x}_i \mid \mathcal{D}) - \log P_{\mathcal{A}}(\mathbf{x}_i \mid \mathcal{D}_{[n] \setminus \{i\}}). \quad (2)$$

The memorization score measures how much more likely an observation is when it is included in the training set compared to when it was not. For example, if $M(\mathcal{A}, \mathcal{D}, i) = 100$, then $P_{\mathcal{A}}(\mathbf{x}_i \mid \mathcal{D}) = \exp(100) \cdot P_{\mathcal{A}}(\mathbf{x}_i \mid \mathcal{D}_{[n] \setminus \{i\}})$. Alternatively, if $M(\mathcal{A}, \mathcal{D}, i) = 0$, then the observation is as likely under the model when it is in the training data as when it is not. We will abbreviate the memorization score as $M_i := M(\mathcal{A}, \mathcal{D}, i)$ when the arguments are clear from context or irrelevant to the discussion.

Estimation. Since it is infeasible to compute the memorization score explicitly for each observation in the training data set, we propose a practical estimator that simplifies the one proposed in [15]. Instead of computing the memorization score M_i for each individual observation $i \in [n]$, we approximate the second term in (2) by randomly sampling index sets \mathcal{I} with $i \in \mathcal{I}$ and constructing training sets $\mathcal{D}_{[n] \setminus \mathcal{I}}$. A particularly effective strategy is to choose the random subsets \mathcal{I} as disjoint subsets of the indices $[n] = \{1, \dots, n\}$, as is done in cross validation. For K folds we have index sets \mathcal{I}_k , $k = 1, \dots, K$, and corresponding training data sets $\mathcal{D}_{[n] \setminus \mathcal{I}_k}$. Training the algorithm \mathcal{A} on these reduced training data sets allows us to compute $p(\mathbf{x}_i \mid \mathcal{D}_{[n] \setminus \mathcal{I}_k}, a_k)$, which can then be used to approximate $P_{\mathcal{A}}(\mathbf{x}_i \mid \mathcal{D}_{[n] \setminus \{i\}})$.

Repeating this process t times, using index sets $\mathcal{I}_{\ell,k}$ for $\ell = 1, \dots, t$ and $k = 1, \dots, K$, yields the sampling estimate

$$P_{\mathcal{A}}(\mathbf{x}_i \mid \mathcal{D}_{[n] \setminus \{i\}}) \approx \frac{1}{t} \sum_{\ell=1}^t \sum_{k=1}^K \mathbb{1}_{i \in \mathcal{I}_{\ell,k}} p(\mathbf{x}_i \mid \mathcal{D}_{[n] \setminus \mathcal{I}_{\ell,k}}, a_{\ell,k}), \quad (3)$$

where $\mathbb{1}_v$ is the indicator function. The first term in the memorization score in (2) can be approximated using the sampling estimate in (1), using a number of repetitions T not necessarily equal to t . Alternatively, we can re-use the models trained for the estimate in (3) and compute

$$P_{\mathcal{A}}(\mathbf{x}_i \mid \mathcal{D}) \approx \frac{1}{t(K-1)} \sum_{\ell=1}^t \sum_{k=1}^K \mathbb{1}_{i \notin \mathcal{I}_{\ell,k}} p(\mathbf{x}_i \mid \mathcal{D}_{[n] \setminus \mathcal{I}_{\ell,k}}, a_{\ell,k}). \quad (4)$$

The latter approach will be more computationally efficient as it allows reusing models trained to estimate (3), but the former is closer to the exact definition of the memorization score and can therefore be expected to yield more accurate results. The estimate of the memorization score is then computed as the difference in the log probabilities in (4) and (3). The number of repetitions t and folds K will in practice be dominated by the available computational resources. The above approach is summarized in Algorithm 1, where log probabilities are used for numerical accuracy.



Figure 2: Observations with low, median, and high memorization scores in the CIFAR-10 data set, when learning the distribution with a convolutional VAE. Memorization scores range from about -180 in the top left of figure (a) to about 900 in the bottom right of figure (c), with a median of 97 .

When is memorization significant? A natural question is what values of the memorization score M_i are significant and of potential concern. The memorization scores can be directly compared between different algorithm settings on the same data set, for instance to understand whether changes in hyperparameters or model architectures increase or decrease memorization. Statistical measures such as the mean, median, and skewness of the memorization score or the location of, say, the 95th percentile, can be informative when quantifying memorization of a particular model on a particular data set, but can not necessarily be compared between data sets. In practice, we also find that the distribution of the memorization score can differ between modes in the data set, such as distinct object classes. This can be understood by considering that the variability of observations of distinct classes likely differs, which affects the likelihood of the objects under the model, and in turn the memorization score. We will return to this question in Section 6.

4 Experiments

We next describe several experiments that advance our understanding of memorization in probabilistic deep generative models, with a focus on the variational autoencoder setting. Additional results are available in Supplement C. Code to reproduce our experiments can be found in an online repository.¹

4.1 Background

We employ the variational autoencoder (VAE) [1, 2] as the probabilistic generative model in our experiments, although it is important to emphasize that the memorization score introduced above is equally applicable to methods such as normalizing flows, diffusion networks, and other generative models that learn a probability density over the input space. The VAE is a latent-variable model, where we model the joint distribution $p_\theta(\mathbf{x}, \mathbf{z})$ of an observation $\mathbf{x} \in \mathcal{X}$ and a latent variable $\mathbf{z} \in \mathcal{Z} = \mathbb{R}^L$. The joint distribution can be factorized as $p_\theta(\mathbf{x}, \mathbf{z}) = p_\theta(\mathbf{x} | \mathbf{z})p(\mathbf{z})$, and in the VAE the prior distribution $p(\mathbf{z})$ is typically assumed to be a standard multivariate Gaussian. The posterior distribution $p_\theta(\mathbf{z} | \mathbf{x})$ is generally intractable, so it is approximated using an inference model, or *encoder*, $q_\phi(\mathbf{z} | \mathbf{x})$. Analogously, the recognition model $p_\theta(\mathbf{x} | \mathbf{z})$ is often referred to as the *decoder*. The VAE is trained by maximizing the lower bound on the evidence (ELBO), see (6), since

$$\log p_\theta(\mathbf{x}) \geq \mathbb{E}_{q_\phi(\mathbf{z} | \mathbf{x})} [\log p_\theta(\mathbf{x}, \mathbf{z}) - \log q_\phi(\mathbf{z} | \mathbf{x})] \quad (5)$$

$$= -D_{\text{KL}}(q_\phi(\mathbf{z} | \mathbf{x}) \| p(\mathbf{z})) + \mathbb{E}_{q_\phi(\mathbf{z} | \mathbf{x})} [\log p_\theta(\mathbf{x} | \mathbf{z})], \quad (6)$$

with $D_{\text{KL}}(\cdot \| \cdot)$ the Kullback-Leibler (KL) divergence [41]. By choosing a simple distribution for the encoder $q_\phi(\mathbf{z} | \mathbf{x})$, such as a multivariate Gaussian, the KL divergence has a closed-form expression, resulting in an efficient training algorithm.

We use importance sampling on the decoder [42] to approximate $\log p_\theta(\mathbf{x}_i)$ for the computation of the memorization score, and focus on the MNIST [43], CIFAR-10 [44], and CelebA [45] data sets. We use a fully connected encoder and decoder for MNIST and employ convolutional architectures for CIFAR-10 and CelebA. For the optimization we use Adam [46] and we implement all models in PyTorch [47]. The memorization score is estimated using $t = 10$ repetitions and $K = 10$ folds. Additional details of the experimental setup and model architectures can be found in Supplement B.

¹See: <https://github.com/alan-turing-institute/memorization>.

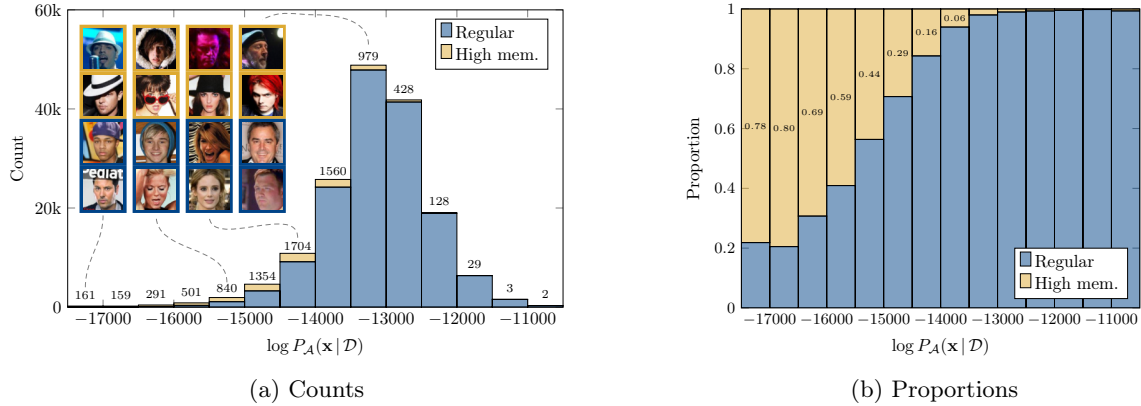


Figure 3: In (a) we show a histogram of the number of highly memorized (yellow) and regular (blue) observations for bins of the log probability under a VAE model trained on the CelebA data set. The numbers above the bars correspond to the number of highly memorized observations in each bin. Randomly selected training observations from several bins are shown as well, with dashed lines illustrating the bin where the images in a particular column can be found. Images with a yellow frame are highly memorized whereas those with a blue frame have low memorization scores. Figure (b) shows the *proportion* of highly memorized and regular observations for each bin.

4.2 Results

We first explore memorization qualitatively. Figure 2 shows examples of observations with low, median, and high memorization scores in the VAE model trained on CIFAR-10. While some of the highly-memorized observations may stand out as odd to a human observer, others appear not unlike those that receive a low memorization score. This shows that the kind of observations that are highly memorized in a particular model may be counterintuitive, and are not necessarily visually anomalous.

If highly memorized observations are always given a low probability when they are included in the training data, then it would be straightforward to dismiss them as outliers that the model recognizes as such. However, we find that this is not universally the case for highly memorized observations, and a sizable proportion of them are likely *only* when they are included in the training data. If we consider observations with the 5% highest memorization scores to be “highly memorized”, then we can check how many of these observations are considered likely by the model when they are included in the training data. Figure 3a shows the number of highly memorized and “regular” observations for bins of the log probability under the VAE model for CelebA, as well as example observations from both groups for different bins. Moreover, Figure 3b shows the proportion of highly memorized observations in each of the bins of the log probability under the model. While the latter figure shows that observations with low probability are *more likely* to be memorized, the former shows that a considerable proportion of highly memorized observations are *as likely as regular observations* when they are included in the training set. Indeed, more than half the highly memorized observations fall within the central 90% of log probability values (i.e. with $\log P_A(\mathbf{x} | \mathcal{D}) \in [-14500, -12000]$).

The memorization score can be a useful diagnostic tool to evaluate the effect of different hyperparameter settings and model architectures. For example, in Figure 4c we illustrate the distribution of the memorization score for two different learning rates in the VAE on the MNIST data set, and we show the train and test set losses during training in Figure 4a. With a learning rate of $\eta = 10^{-3}$ (blue curves), a clear generalization gap can be seen in the loss curves, indicating the start of overtraining (note the test loss has not yet started to *increase*). This generalization gap disappears when training with the smaller learning rate of $\eta = 10^{-4}$ (yellow curves). The absence of a generalization gap is sometimes used as evidence for the absence of overfitting and memorization [48], but the distribution of the memorization scores for $\eta = 10^{-4}$ in Figure 4c shows that this is insufficient. While the memorization scores are *reduced* by lowering the learning rate, high memorization can still occur. In fact, the largest memorization score for $\eta = 10^{-4}$ is about 80, and represents a shift from a far outlier when the observation is absent from the training data to a central inlier when it is present.²

²For this particular observation, $\log P_A(\mathbf{x}_i | \mathcal{D}_{[n] \setminus \{i\}}) \approx -178$ when the observation is excluded from the training data, and $\log P_A(\mathbf{x}_i | \mathcal{D}) \approx -97$ when it is included, and the latter value is approximately equal to the average log probability of the other observations with the same digit.

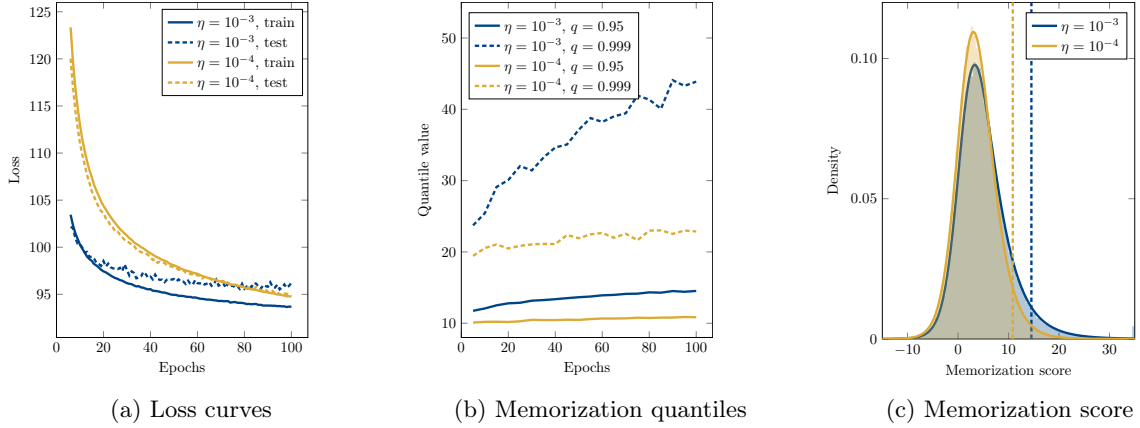


Figure 4: Loss curves, memorization score quantiles, and memorization score distributions for a VAE trained on MNIST with different learning rates, $\eta = 10^{-3}$ (blue) and $\eta = 10^{-4}$ (yellow). In (c) the vertical lines mark the 95th percentile of the memorization scores, and the axes are cropped for clarity (the maximum memorization score for $\eta = 10^{-3}$ is about 210 and for $\eta = 10^{-4}$ it is about 80).

4.3 Memorization during training

To continue on the relation between memorization and overtraining, we look at how the memorization score evolves during training. In Figure 4b we show the 0.95 and 0.999 quantiles of the memorization score for the VAE trained on MNIST using two different learning rates. The quantiles are chosen such that they show the memorization score for the highly memorized observations. For both learning rates we see that the memorization score increases during training, as can be expected. However we also see that for the larger learning rate of $\eta = 10^{-3}$ the memorization score is already considerable before the generalization gap in Figure 4a appears. This is additional evidence that determining memorization by the generalization gap is insufficient, and implies that early stopping would not fully alleviate memorization. Moreover, we see that the rate of increase for the peak memorization quantiles slows down with more training, which suggests that the memorization score stabilizes and does not keep increasing with the training epochs. This is reminiscent of [19], who demonstrated that their metric for memorization in language models peaks when the test loss starts to increase. The difference is that here memorization appears to stabilize even before this happens.

4.4 Nearest Neighbors

As discussed in the introduction, nearest neighbor illustrations are commonly used to argue that no memorization is present in the model. Moreover, hypothesis tests and evaluation metrics have been proposed that measure memorization using distances between observations and samples [24, 25]. Because of the prevalence of nearest neighbor tests for memorization, we next demonstrate the relationship between our proposed memorization score and a nearest neighbor metric.

As an example of a nearest neighbor test, we look at the relative distance of observations from the training set to generated samples and observations from the validation set. Let $\mathcal{S} \subseteq \mathcal{X}$ be a set of samples from the model and let $\mathcal{V} \subseteq \mathcal{X}$ be the validation set, with $|\mathcal{S}| = |\mathcal{V}|$. Denote by $d : \mathcal{X} \times \mathcal{X}$ a distance metric, which we'll choose here to be the Euclidean distance between images in pixel space after downsampling by a factor of 2. For all \mathbf{x}_i in the training set \mathcal{D} , we then compute the ratio between the closest distance to a member of the validation set and a member of the sample set,

$$\rho_i = \frac{\min_{\mathbf{x} \in \mathcal{V}} d(\mathbf{x}_i, \mathbf{x})}{\min_{\mathbf{x} \in \mathcal{S}} d(\mathbf{x}_i, \mathbf{x})}. \quad (7)$$

If $\rho_i > 1$, then the nearest neighbor of \mathbf{x}_i in the sample set is closer than the nearest neighbor in the validation set, and vice versa. Investigating if the average ratio for a set of observations differs significantly from 1 is an example of using hypothesis testing approaches to measure memorization.

Figure 5 illustrates the relationship between ρ_i and the memorization score M_i . We see that in general there is no strong correlation between the two score functions, which can be explained by the fact that they measure different quantities. While the memorization score directly measures how much the model relies on the presence of \mathbf{x}_i for the local probability density, nearest neighbor methods test how “close”

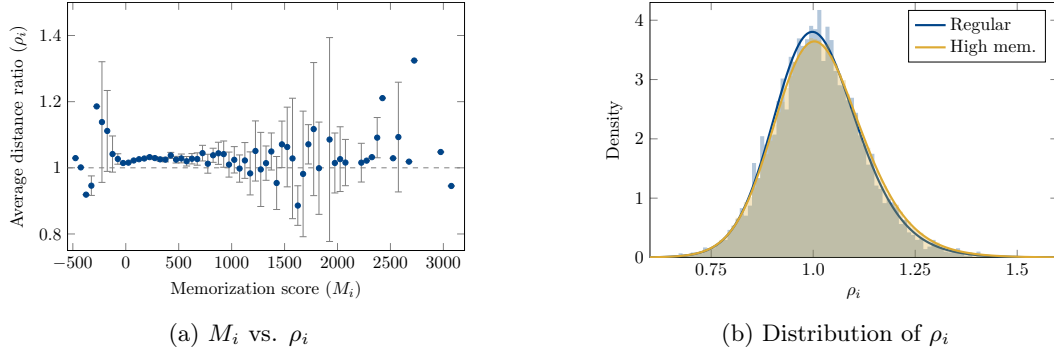


Figure 5: Illustration of the nearest neighbor distance ratio in (7) compared to the memorization score for a VAE trained on CelebA. Due to the large number of observations, we present the average of ρ_i for bins of the memorization score of width 50, and show error bars representing the confidence interval of the standard error of the mean of distance ratio measurements in each bin. The horizontal axis in figure (a) trims off one observation at $M_i \approx 6500$ for clarity. Figure (b) shows the distribution of the distance ratio for observations with a high memorization score (top 5%) and the regular ones.

samples from the model are to the training or validation data. They thus require a meaningful distance metric (which is non-trivial for high-dimensional data) and are subject to variability in the sample and validation sets. We therefore argue that while nearest neighbor examples and hypothesis tests can be informative and may detect global memorization, to understand memorization at an instance level the proposed memorization score is to be preferred.

5 Mitigation Strategies

We describe several strategies that can be used to mitigate memorization in probabilistic generative models. First, the memorization score can be directly related to the concept of Differential Privacy (DP) [49, 50]. Note that the memorization score in (2) can be rewritten as

$$P_{\mathcal{A}}(\mathbf{x}_i | \mathcal{D}) = \exp(M(\mathcal{A}, \mathcal{D}, i)) P_{\mathcal{A}}(\mathbf{x}_i | \mathcal{D}_{[n] \setminus \{i\}}), \quad (8)$$

and recall that a randomized algorithm \mathcal{A} is ϵ -differentially private if for *all* data sets $\mathcal{D}_1, \mathcal{D}_2$ that differ in only one element the following inequality holds

$$P_{\mathcal{A}}(\mathcal{W} | \mathcal{D}_1) \leq \exp(\epsilon) P_{\mathcal{A}}(\mathcal{W} | \mathcal{D}_2), \quad \forall \mathcal{W} \subseteq \mathcal{X}. \quad (9)$$

Since this must hold for all subsets \mathcal{W} of \mathcal{X} , it must also hold for the case where $\mathcal{W} = \{\mathbf{x}_i\}$. Moreover, when \mathbf{x}_i is removed from \mathcal{D} it can be expected that the largest change in density occurs at \mathbf{x}_i . It then follows that the memorization score can be bounded by employing ϵ -DP estimation techniques when training the generative model, as this will guarantee that $M_i \leq \epsilon, \forall i$. The converse is however not true: observing a maximum memorization score of $M_i = \epsilon$ for a particular model does not imply that the model is also ϵ -DP. This connection of the memorization score to differential privacy offers additional support for the proposed formulation of the memorization score.

An alternative approach to limit memorization is to explicitly incorporate an outlier component in the model, which would enable it to effectively ignore atypical observations when learning the probability density. This technique has been previously used to handle outliers in factorial switching models [51] and to perform outlier detection in VAEs for tabular data [52]. The intuition is that by including a model component with broad support but low probability (such as a Gaussian with high variance), the log probability for atypical observations will be small whether they are included in the training data or not, resulting in a low memorization score. Other approaches such as using robust divergence measures instead of the KL-divergence in VAEs [53], might also be able to alleviate memorization.

6 Discussion

We have introduced a principled formulation of a memorization score for probabilistic generative models. The memorization score directly measures the impact of removing an observation on the model, and

thereby allows us to quantify the degree to which the model has memorized it. We explored how the memorization score evolves during training and how it relates to typical nearest neighbor tests, and we have shown that highly memorized observations are not necessarily unlikely under the model. A question that requires further study is what constitutes a “high” memorization score on a particular data set. One of the main difficulties with this is that density estimates returned by a model, and thus probability differences, are not necessarily comparable between data sets [32]. We expect that future work will focus on this important question, and suggest that inspiration may be taken from work on choosing ϵ in differential privacy [54, 55]. Improving the efficiency of the estimator is also considered an important topic for future work.

If we want diversity in the samples created by generative models, then the model will have to learn to generalize to regions of the data manifold that are not well represented in the input data. Whether this is achieved by extrapolating from other regions of the space or fails due to memorization is an important question. Our work thus contributes to the ongoing effort to understand the balance between memorization and generalization in deep generative neural networks.

Acknowledgments

This work was supported in part by The Alan Turing Institute under EPSRC grant EP/N510129/1.

References

- [1] Kingma, D. P. and Welling, M. Auto-encoding Variational Bayes. In *2nd International Conference on Learning Representations*, edited by Y. Bengio and Y. LeCun, 2014.
- [2] Rezende, D. J., Mohamed, S., and Wierstra, D. Stochastic Backpropagation and Approximate Inference in Deep Generative Models. In *Proceedings of the 31st International Conference on Machine Learning*, edited by E. P. Xing and T. Jebara, volume 32 of *Proceedings of Machine Learning Research*, pp. 1278–1286. PMLR, Beijing, China, 2014.
- [3] Goodfellow, I., Pouget-Abadie, J., Mirza, M., Xu, B., Warde-Farley, D., Ozair, S., Courville, A., and Bengio, Y. Generative Adversarial Nets. In *Advances in Neural Information Processing Systems*, edited by Z. Ghahramani, M. Welling, C. Cortes, N. Lawrence, and K. Q. Weinberger, volume 27. Curran Associates, Inc., 2014.
- [4] Tabak, E. G. and Turner, C. V. A Family of Nonparametric Density Estimation Algorithms. *Communications on Pure and Applied Mathematics*, 66(2):145–164, 2013.
- [5] Rezende, D. and Mohamed, S. Variational Inference with Normalizing Flows. In *Proceedings of the 32nd International Conference on Machine Learning*, edited by F. R. Bach and D. Blei, volume 37 of *Proceedings of Machine Learning Research*, pp. 1530–1538. PMLR, Lille, France, 2015.
- [6] Sohl-Dickstein, J., Weiss, E., Maheswaranathan, N., and Ganguli, S. Deep Unsupervised Learning using Nonequilibrium Thermodynamics. In *Proceedings of the 32nd International Conference on Machine Learning*, edited by F. R. Bach and D. Blei, volume 37 of *Proceedings of Machine Learning Research*, pp. 2256–2265. PMLR, Lille, France, 2015.
- [7] Theis, L., van den Oord, A., and Bethge, M. A Note on the Evaluation of Generative Models. In *4th International Conference on Learning Representations*, edited by Y. Bengio and Y. LeCun, 2016.
- [8] Karras, T., Aila, T., Laine, S., and Lehtinen, J. Progressive Growing of GANs for Improved Quality, Stability, and Variation. In *6th International Conference on Learning Representations*, 2018.
- [9] Brock, A., Donahue, J., and Simonyan, K. Large Scale GAN Training for High Fidelity Natural Image Synthesis. In *7th International Conference on Learning Representations*, 2019.
- [10] Vahdat, A. and Kautz, J. NVAE: A Deep Hierarchical Variational Autoencoder. In *Advances in Neural Information Processing Systems*, edited by H. Larochelle, M. Ranzato, R. Hadsell, M. F. Balcan, and H. Lin, volume 33, pp. 19667–19679. Curran Associates, Inc., 2020.
- [11] Barz, B. and Denzler, J. Do We Train on Test Data? Purging CIFAR of Near-Duplicates. *Journal of Imaging*, 6(6):41, 2020.

- [12] Rosenblatt, M. Remarks on Some Nonparametric Estimates of a Density Function. *The Annals of Mathematical Statistics*, 27(3):832 – 837, 1956.
- [13] Parzen, E. On Estimation of a Probability Density Function and Mode. *The Annals of Mathematical Statistics*, 33(3):1065 – 1076, 1962.
- [14] Feldman, V. Does Learning Require Memorization? A Short Tale about a Long Tail. *arXiv preprint arXiv:1906.05271*, 2019.
- [15] Feldman, V. and Zhang, C. What Neural Networks Memorize and Why: Discovering the Long Tail via Influence Estimation. In *Advances in Neural Information Processing Systems*, edited by H. Larochelle, M. Ranzato, R. Hadsell, M. F. Balcan, and H. Lin, volume 33, pp. 2881–2891. Curran Associates, Inc., 2020.
- [16] Zhang, C., Bengio, S., Hardt, M., Recht, B., and Vinyals, O. Understanding Deep Learning Requires Rethinking Generalization. In *5th International Conference on Learning Representations*, 2017.
- [17] Arpit, D., Jastrzebski, S., Ballas, N., Krueger, D., Bengio, E., Kanwal, M. S., Maharaj, T., Fischer, A., Courville, A., Bengio, Y., and Lacoste-Julien, S. A Closer Look at Memorization in Deep Networks. In *Proceedings of the 34th International Conference on Machine Learning*, edited by D. Precup and Y. W. Teh, volume 70, pp. 233–242, 2017.
- [18] Stephenson, C., Padhy, S., Ganesh, A., Hui, Y., Tang, H., and Chung, S. On the Geometry of Generalization and Memorization in Deep Neural Networks. In *9th International Conference on Learning Representations*, 2021.
- [19] Carlini, N., Liu, C., Erlingsson, Ú., Kos, J., and Song, D. The Secret Sharer: Evaluating and Testing Unintended Memorization in Neural Networks. In *28th USENIX Security Symposium*, pp. 267–284, 2019.
- [20] Jiang, Z., Zhang, C., Talwar, K., and Mozer, M. C. Characterizing Structural Regularities of Labeled Data in Overparameterized Models. *arXiv preprint arXiv:2002.03206*, 2020.
- [21] Liu, S., Niles-Weed, J., Razavian, N., and Fernandez-Granda, C. Early-Learning Regularization Prevents Memorization of Noisy Labels. In *Advances in Neural Information Processing Systems*, edited by H. Larochelle, M. Ranzato, R. Hadsell, M. F. Balcan, and H. Lin, volume 33, pp. 20331–20342. Curran Associates, Inc., 2020.
- [22] Xia, X., Liu, T., Han, B., Gong, C., Wang, N., Ge, Z., and Chang, Y. Robust Early-Learning: Hindering the Memorization of Noisy Labels. In *9th International Conference on Learning Representations*, 2021.
- [23] Lopez-Paz, D. and Oquab, M. Revisiting Classifier Two-Sample Tests. In *5th International Conference on Learning Representations*, 2017.
- [24] Xu, Q., Huang, G., Yuan, Y., Guo, C., Sun, Y., Wu, F., and Weinberger, K. Q. An Empirical Study on Evaluation Metrics of Generative Adversarial Networks. *arXiv preprint arXiv:1806.07755*, 2018.
- [25] Meehan, C., Chaudhuri, K., and Dasgupta, S. A Non-Parametric Test to Detect Data-Copying in Generative Models. In *Proceedings of the 23rd International Conference on Artificial Intelligence and Statistics*, edited by S. Chiappa and R. Calandra, volume 108 of *Proceedings of Machine Learning Research*, pp. 3546–3556. PMLR, 2020.
- [26] Fredrikson, M., Jha, S., and Ristenpart, T. Model Inversion Attacks that Exploit Confidence Information and Basic Countermeasures. In *Proceedings of the 22nd ACM SIGSAC Conference on Computer and Communications Security*, pp. 1322–1333, 2015.
- [27] Shokri, R., Stronati, M., Song, C., and Shmatikov, V. Membership Inference Attacks against Machine Learning Models. In *2017 IEEE Symposium on Security and Privacy*, pp. 3–18. IEEE, 2017.
- [28] Hitaj, B., Ateniese, G., and Perez-Cruz, F. Deep Models Under the GAN: Information Leakage from Collaborative Deep Learning. In *Proceedings of the 2017 ACM SIGSAC Conference on Computer and Communications Security*, pp. 603–618, 2017.

- [29] Hayes, J., Melis, L., Danezis, G., and De Cristofaro, E. LOGAN: Membership Inference Attacks Against Generative Models. In *Proceedings on Privacy Enhancing Technologies*, 1, pp. 133–152, 2018.
- [30] Webster, R., Rabin, J., Simon, L., and Jurie, F. Detecting Overfitting of Deep Generative Networks via Latent Recovery. In *Proceedings of the IEEE/CVF Conference on Computer Vision and Pattern Recognition*, pp. 11273–11282, 2019.
- [31] Arora, S., Risteski, A., and Zhang, Y. Do GANs Learn the Distribution? Some Theory and Empirics. In *6th International Conference on Learning Representations*, 2018.
- [32] Nalisnick, E., Matsukawa, A., Teh, Y. W., Gorur, D., and Lakshminarayanan, B. Do Deep Generative Models Know What They Don’t Know? In *7th International Conference on Learning Representations*, 2019.
- [33] Salimans, T., Goodfellow, I., Zaremba, W., Cheun, V., Radford, A., and Chen, X. Improved Techniques for Training GANs. In *Advances in Neural Information Processing Systems*, edited by D. D. Lee, M. Sugiyama, U. V. Luxburg, I. Guyon, and R. Garnett, volume 29, pp. 2234–2242. Curran Associates, Inc., 2016.
- [34] Heusel, M., Ramsauer, H., Unterthiner, T., Nessler, B., and Hochreiter, S. GANs Trained by a Two Time-Scale Update Rule Converge to a Local Nash Equilibrium. In *Advances in Neural Information Processing Systems*, edited by I. Guyon, U. V. Luxburg, S. Bengio, H. Wallach, R. Fergus, S. Vishwanathan, and R. Garnett, volume 30. Curran Associates, Inc., 2017.
- [35] Gulrajani, I., Raffel, C., and Metz, L. Towards GAN Benchmarks Which Require Generalization. In *7th International Conference on Learning Representations*, 2019.
- [36] Hampel, F. R. The Influence Curve and Its Role in Robust Estimation. *Journal of the American Statistical Association*, 69(346):383–393, 1974.
- [37] Cook, R. D. and Weisberg, S. Characterizations of an Empirical Influence Function for Detecting Influential Cases in Regression. *Technometrics*, 22(4):495–508, 1980.
- [38] Koh, P. W. and Liang, P. Understanding Black-box Predictions via Influence Functions. In *Proceedings of the 34th International Conference on Machine Learning*, edited by D. Precup and Y. W. Teh, volume 70, pp. 1885–1894, 2017.
- [39] Terashita, N., Ohashi, H., Nonaka, Y., and Kanemaru, T. Influence Estimation for Generative Adversarial Networks. In *9th International Conference on Learning Representations*, 2021.
- [40] Basu, S., Pope, P., and Feizi, S. Influence Functions in Deep Learning Are Fragile. In *9th International Conference on Learning Representations*, 2021.
- [41] Kullback, S. and Leibler, R. A. On Information and Sufficiency. *The Annals of Mathematical Statistics*, 22(1):79–86, 1951.
- [42] Burda, Y., Grosse, R. B., and Salakhutdinov, R. Importance Weighted Autoencoders. In *4th International Conference on Learning Representations*, edited by Y. Bengio and Y. LeCun, 2016.
- [43] LeCun, Y., Cortes, C., and Burges, C. J. C. The MNIST Database of Handwritten Digits, 1998.
- [44] Krizhevsky, A. *Learning Multiple Layers of Features from Tiny Images*. Master’s thesis, University of Toronto, 2009.
- [45] Liu, Z., Luo, P., Wang, X., and Tang, X. Deep Learning Face Attributes in the Wild. In *Proceedings of International Conference on Computer Vision*, 2015.
- [46] Kingma, D. P. and Ba, J. Adam: A Method for Stochastic Optimization. In *3rd International Conference on Learning Representations*, edited by Y. Bengio and Y. LeCun, 2015.
- [47] Paszke, A., Gross, S., Massa, F., Lerer, A., Bradbury, J., Chanan, G., Killeen, T., Lin, Z., Gimelshein, N., Antiga, L., Desmaison, A., Köpf, A., Yang, E., DeVito, Z., Raison, M., Tejani, A., Chilamkurthy, S., Steiner, B., Fang, L., Bai, J., and Chintala, S. PyTorch: An Imperative Style, High-Performance Deep Learning Library. In *Advances in Neural Information Processing Systems*, edited by H. Wallach, H. Larochelle, A. Beygelzimer, F. d’Alché Buc, E. B. Fox, and R. Garnett, volume 32. Curran Associates, Inc., 2019.

- [48] Wu, Y., Burda, Y., Salakhutdinov, R., and Grosse, R. B. On the Quantitative Analysis of Decoder-Based Generative Models. In *5th International Conference on Learning Representations*, 2017.
- [49] Dwork, C., McSherry, F., Nissim, K., and Smith, A. Calibrating Noise to Sensitivity in Private Data Analysis. In *Theory of Cryptography Conference*, pp. 265–284. Springer, 2006.
- [50] Dwork, C. and Roth, A. The Algorithmic Foundations of Differential Privacy. *Foundations and Trends in Theoretical Computer Science*, 9(3–4):211–407, 2014.
- [51] Quinn, J. A., Williams, C. K. I., and McIntosh, N. Factorial Switching Linear Dynamical Systems Applied to Physiological Condition Monitoring. *IEEE Transactions on Pattern Analysis and Machine Intelligence*, 31(9):1537–1551, 2009.
- [52] Eduardo, S., Nazábal, A., Williams, C. K. I., and Sutton, C. Robust Variational Autoencoders for Outlier Detection and Repair of Mixed-Type Data. In *International Conference on Artificial Intelligence and Statistics*, pp. 4056–4066. PMLR, 2020.
- [53] Akrami, H., Joshi, A. A., Li, J., Aydore, S., and Leahy, R. M. Robust Variational Autoencoder. *arXiv preprint arXiv:1905.09961*, 2019.
- [54] Lee, J. and Clifton, C. How Much is Enough? Choosing ϵ for Differential Privacy. In *International Conference on Information Security*, pp. 325–340. Springer, 2011.
- [55] Hsu, J., Gaboardi, M., Haeberlen, A., Khanna, S., Narayan, A., Pierce, B. C., and Roth, A. Differential Privacy: An Economic Method for Choosing Epsilon. In *2014 IEEE 27th Computer Security Foundations Symposium*, pp. 398–410. IEEE, 2014.
- [56] Ho, J., Jain, A., and Abbeel, P. Denoising Diffusion Probabilistic Models. In *Advances in Neural Information Processing Systems*, edited by H. Larochelle, M. Ranzato, R. Hadsell, M. F. Balcan, and H. Lin, volume 33. Curran Associates, Inc., 2020.
- [57] Song, Y., Sohl-Dickstein, J., Kingma, D. P., Kumar, A., Ermon, S., and Poole, B. Score-Based Generative Modeling through Stochastic Differential Equations. In *9th International Conference on Learning Representations*, 2021.
- [58] Salakhutdinov, R. and Murray, I. On the Quantitative Analysis of Deep Belief Networks. In *Proceedings of the 25th International Conference on Machine Learning*, edited by A. McCallum and S. Roweis, pp. 872–879. Omnipress, 2008.
- [59] Nair, V. and Hinton, G. E. Rectified Linear Units Improve Restricted Boltzmann Machines. In *Proceedings of the 27th International Conference on Machine Learning*, edited by J. Fürnkranz and T. Joachims, pp. 807–814. Omnipress, 2010.
- [60] Uria, B., Murray, I., and Larochelle, H. RNADE: The Real-Valued Neural Autoregressive Density-Estimator. In *Advances in Neural Information Processing Systems*, edited by C. J. C. Burges, L. Bottou, M. Welling, Z. Ghahramani, and K. Q. Weinberger, volume 26, pp. 2175–2183. Curran Associates, Inc., 2013.
- [61] Papamakarios, G., Pavlakou, T., and Murray, I. Masked Autoregressive Flow for Density Estimation. In *Advances in Neural Information Processing Systems*, edited by I. Guyon, U. V. Luxburg, S. Bengio, H. Wallach, R. Fergus, S. Vishwanathan, and R. Garnett, volume 30. Curran Associates, Inc., 2017.
- [62] Radford, A., Metz, L., and Chintala, S. Unsupervised Representation Learning with Deep Convolutional Generative Adversarial Networks. In *4th International Conference on Learning Representations*, edited by Y. Bengio and Y. LeCun, 2016.
- [63] Ioffe, S. and Szegedy, C. Batch Normalization: Accelerating Deep Network Training by Reducing Internal Covariate Shift. In *Proceedings of the 32nd International Conference on Machine Learning*, edited by F. R. Bach and D. Blei, volume 37 of *Proceedings of Machine Learning Research*, pp. 448–456. PMLR, Lille, France, 2015.
- [64] Maas, A. L., Hannun, A. Y., and Ng, A. Y. Rectifier Nonlinearities Improve Neural Network Acoustic Models. In *Proceedings of the 30th International Conference on Machine Learning*, edited by S. Dasgupta and D. McAllester, volume 28 of *Proceedings of Machine Learning Research*. PMLR, 2013.

Appendix

A Memorized observations in recent generative models

While experimenting with the proposed memorization score on CIFAR-10 [44], we noticed that the images of automobiles shown in Figure 6 are present in the training set multiple times (with slight variation). We subsequently spotted these images in the illustrations of generated samples in [56] (Figure 13, example (a) can be seen twice) and [57] (Figure 11 and Figure 13, truck class). These works are recently proposed probabilistic generative models that achieve impressive performance on sample quality metrics such as the inception score (IS) [33] and the Fréchet inception distance (FID) [34], and also achieve high log likelihoods. However, the fact that we were able to serendipitously spot images from the training set in the generated samples might suggest that some unintended memorization occurs in these models. We do not know if there are other images in the presented samples that occur in the training data. Of course, spotting near duplicates of training observations is only possible because these models yield realistic samples. As we argue in the main text and as has been shown by previous works [30, 35], quality metrics such as IS and FID do not detect memorization.

We emphasize that this evidence is presented mainly to support the notion that (unintended) memorization can occur in probabilistic deep generative models, and to provide additional motivation for understanding and quantifying when and how memorization arises, which is the focus of our work.

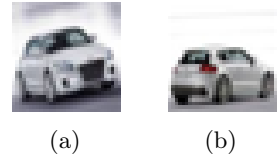


Figure 6: Examples of images from the CIFAR-10 training set that were spotted in illustrations of samples from the model in recent work on generative models.

B Experimental Details

This section describes additional details of the data sets, model architectures, and experimental setup.

B.1 Datasets

We use the MNIST [43], CIFAR-10 [44], and CelebA [45] data sets, which are widely used and are freely available for research purposes (although to the best of our knowledge explicit licenses are not available). For MNIST we binarize the images dynamically during training by considering each grayscale pixel value as the parameter of an independent Bernoulli variable, as is common [10, 58]. Images in all data sets are resized to 32×32 pixels for efficiency and ease of implementation. CIFAR-10 contains color images from 10 different categories and does not require further preprocessing. CelebA contains potentially identifiable images of faces of celebrities sourced from publicly available images on the Internet. We used the predefined cropping function of [10] to center the face region. For CIFAR-10 and CelebA we used random horizontal flips during training as data augmentation. All data sets have predefined train and test sets, and CelebA additionally has a validation set. We mainly used the training sets in the experiments, with the exception of the experiments for Figure 4a, which uses the MNIST test set, and the experiments in Section 4.4, which use the CelebA validation set.

B.2 Model Architectures

Let L denote the size of the latent space and recall that $\mathbf{x} \in \mathcal{X} \subseteq \mathbb{R}^D$. For all experiments we used a Gaussian encoder with a learned diagonal covariance matrix, $q_\phi(\mathbf{z} | \mathbf{x}) = \mathcal{N}(\mathbf{z}; \boldsymbol{\mu}_\phi(\mathbf{x}), \text{diag}(\boldsymbol{\sigma}_\phi^2(\mathbf{x})))$ and a standard multivariate Gaussian prior on the latent variables, $p(\mathbf{z}) = \mathcal{N}(\mathbf{z}; \mathbf{0}, \mathbf{I}_L)$. As mentioned above we used a dynamically binarized version of the MNIST data set, and therefore used a Bernoulli likelihood for the decoder of the VAE. Both the encoder and decoder used fully connected layers with the ReLU activation on the intermediate layers [59] and a sigmoid activation on the output of the decoder that represents the parameter of the Bernoulli distribution. For MNIST we used $L = 16$. Full details of the model architecture are given in Table 1.

For CIFAR-10 and CelebA we used a Gaussian likelihood for the decoder, employed uniform dequantization on the pixel values [60], and trained the models in logit space following [61]. For both data sets we used an architecture similar to DCGAN [62], consisting of four convolutional blocks in the encoder, each

Table 1: Model architectures used for the experiments. We used fully connected (FC) layers with the ReLU activation for MNIST, with the SIGMOID activation on the decoder. For CIFAR-10 and CelebA we used convolutional layers for the encoder (CONV2D with kernel size 4, stride 2, and padding 1), followed by batch normalization (BN), and the Leaky ReLU activation (LReLU, using slope 0.2). For these data sets the decoder consists of transposed convolution layers (CONVT2D, with kernel size 4, stride 2, and padding 1 except for the layer marked with an asterisk (*), which uses kernel size 2, stride 1, and padding 0 to get the correct output size), followed by batch norm and the ReLU activation. We use the abbreviations $\text{ENCBLOCK}(C_1, C_2) = \text{CONV2D}(C_1, C_2) \rightarrow \text{BN} \rightarrow \text{LEAKYReLU}$ and $\text{DECBLOCK}(C_1, C_2) = \text{CONVT2D}(C_1, C_2) \rightarrow \text{BN} \rightarrow \text{ReLU}$.

Data set	Encoder network	Decoder network	Likelihood ($p_\theta(\mathbf{x} \mathbf{z})$)
MNIST	FC(1024, 512) \rightarrow ReLU \rightarrow FC(512, 256) \rightarrow ReLU \rightarrow FC(256, L), FC(256, L)	FC(L , 256) \rightarrow ReLU \rightarrow FC(256, 512) \rightarrow ReLU \rightarrow FC(512, 1024) \rightarrow SIGMOID	$\mathcal{B}(x_{ij}; \pi_{ij}(\mathbf{z}))$
CIFAR-10	CONV2D(C , F) \rightarrow LReLU \rightarrow ENCBLOCK(F , $2F$) \rightarrow ENCBLOCK($2F$, $4F$) \rightarrow ENCBLOCK($4F$, $8F$) \rightarrow FLATTEN \rightarrow FC($32F$, L), FC($32F$, L)	DECBLOCK*(L , $8F$) \rightarrow DECBLOCK($8F$, $4F$) \rightarrow DECBLOCK($4F$, $2F$) \rightarrow DECBLOCK($2F$, F) \rightarrow CONVT2D(F , $2C$)	$\mathcal{N}(\mathbf{x}; \boldsymbol{\mu}_\theta(\mathbf{z}), \text{diag}(\boldsymbol{\sigma}_\theta(\mathbf{z})))$
CelebA	Same as for CIFAR-10	Same as for CIFAR-10, except final layer uses CONVT2D(F , C)	$\mathcal{N}(\mathbf{x}; \boldsymbol{\mu}_\theta(\mathbf{z}), \gamma_\theta \mathbf{I}_D)$

by batch normalization [63] and the leaky ReLU activation [64], and five transposed convolution blocks in the decoder followed by batch norm and ReLU, see Table 1. For CIFAR-10 the Gaussian likelihood on the decoder was parameterized as $p_\theta(\mathbf{x}|\mathbf{z}) = \mathcal{N}(\mathbf{x}; \boldsymbol{\mu}_\theta(\mathbf{z}), \text{diag}(\boldsymbol{\sigma}_\theta(\mathbf{z})))$ and for CelebA we used the simpler formulation $p_\theta(\mathbf{x}|\mathbf{z}) = \mathcal{N}(\mathbf{x}; \boldsymbol{\mu}_\theta(\mathbf{z}), \gamma_\theta \mathbf{I}_D)$ with a learned parameter γ_θ , as the more general decoder was unnecessary. For both CIFAR-10 and CelebA the number of input channels is $C = 3$ and we used $L = 64$ and $L = 32$, respectively. For the convolutional networks the feature map multiplier was set to $F = 32$ (see Table 1).

B.3 Training details

We used Adam [46] to optimize the parameters of the model with learning rate $\eta = 10^{-3}$ for the main experiments and $\eta = 10^{-4}$ for the experiments on MNIST in Section 4.2. We used a batch size of 64 and left the remaining parameters for Adam at their default values in PyTorch [47]. For both MNIST and CIFAR-10 we trained for 100 epochs, and used 50 epochs for CelebA. These settings were determined by taking into consideration the available computational resources and aimed to avoid overtraining. These parameter settings were determined through some preliminary experimentation and were not extensively optimized. Experiments were conducted on a desktop machine running Arch Linux, using an NVIDIA GeForce GTX 1660 SUPER GPU, 32GB of RAM, and an AMD Ryzen 5 3600 processor. Total wall-clock time was about 200 hours for the main results, excluding preliminary experimentation. Electricity needed for the experiments came from carbon-free sources.

As mentioned in the main text, importance sampling was used to approximate $p(\mathbf{x})$, such that

$$p(\mathbf{x}) \approx \frac{1}{N} \sum_{l=1}^N \frac{p_\theta(\mathbf{x}|\mathbf{z}_l)p(\mathbf{z}_l)}{q_\phi(\mathbf{z}_l|\mathbf{x})}, \quad \mathbf{z}_l \sim q_\phi(\mathbf{z}|\mathbf{x}). \quad (10)$$

This was computed in log space for numerical accuracy. For MNIST we used $N = 256$ and for CIFAR-10 and CelebA we used $N = 128$ samples.

C Additional Results

Below we show additional results that confirm the findings presented in the main text for different data sets.

C.1 Qualitative Illustrations

In Figures 7, 8, and 9 we illustrate observations with low, median, and high memorization scores for a VAE trained on MNIST using $\eta = 10^{-3}$, MNIST using $\eta = 10^{-4}$, and CelebA, respectively. As can be seen from the figures and as discussed in the main text in Section 4.2, while some of the highly memorized observations have visual anomalies, others are not unlike those that receive low memorization scores. For instance, for the VAE trained on MNIST with learning rate $\eta = 10^{-4}$, we see that images from both the low and high memorization groups have active pixels that are not part of the digit (compare e.g. the images of 9s on the middle of the bottom rows of Figure 8a and Figure 8c).

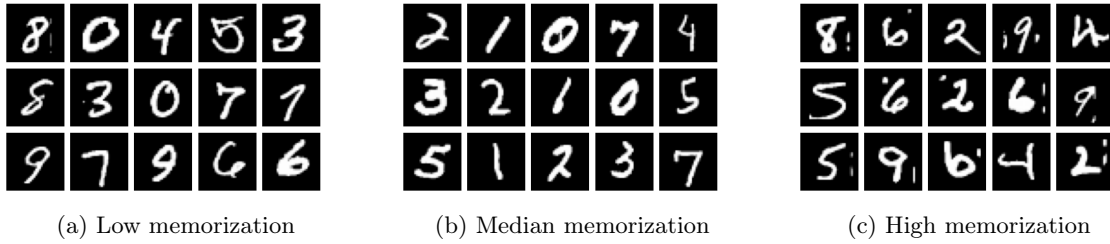


Figure 7: Observations with low, median, and high memorization scores in the MNIST data set, for a VAE trained using learning rate $\eta = 10^{-3}$. Memorization scores range from about -18 in the top left of figure (a) to about 200 in the bottom right of figure (c), with a median of 4.4.

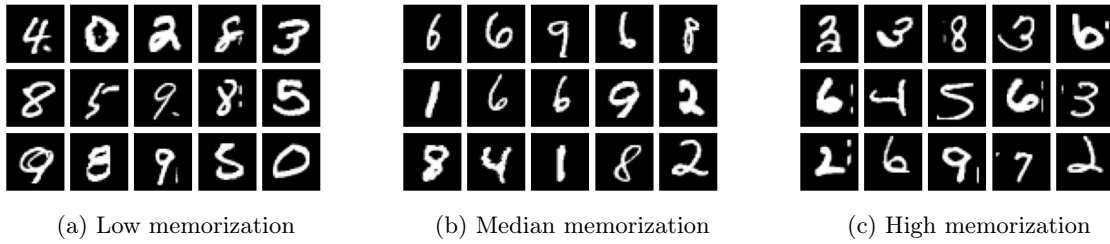


Figure 8: Observations with low, median, and high memorization scores in the MNIST data set, for a VAE trained using learning rate $\eta = 10^{-4}$. Memorization scores range from about -13 in the top left of figure (a) to about 80 in the bottom right of figure (c), with a median of 3.5.

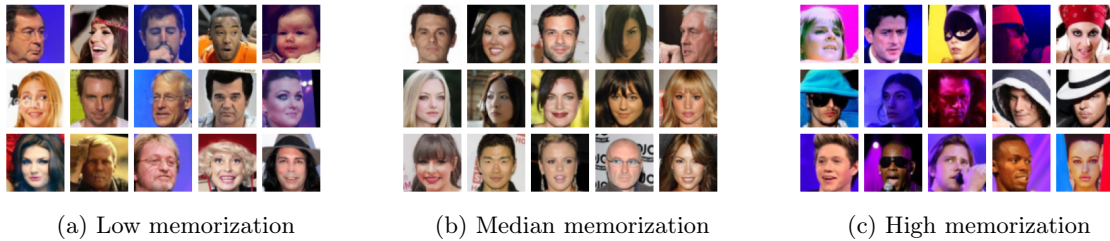


Figure 9: Observations with low, median, and high memorization scores in the CelebA data set when the density is learned using a convolutional VAE. Memorization scores range from about -450 in the top left of figure (a) to about 6500 in the bottom right of figure (c), with a median of about 60.

C.2 Outliers vs. Memorization

Figures 10 and 11 replicate the experiments shown in Figure 3 in the main text for the VAE trained on the MNIST data set using two different learning rates. We again see that relatively high memorization is

not exclusive to observations that receive a low probability under the model. Note that for this particular data set the density estimated by the VAE is slightly multimodal, with the peak in density for higher values of $\log P_A(\mathbf{x} | \mathcal{D})$ corresponding to observations for digit 1.

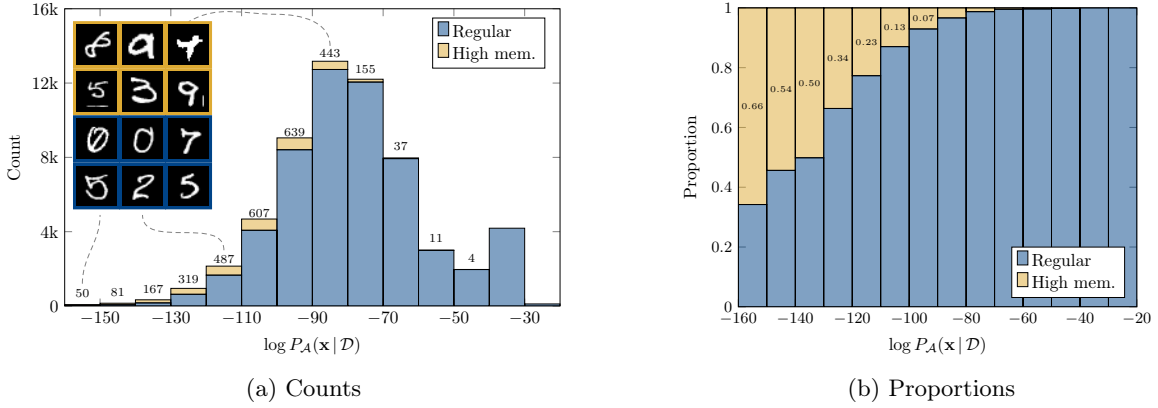


Figure 10: In (a) we show a histogram of the number of highly memorized (yellow) and regular (blue) observations for bins of the log probability under a VAE model trained on the MNIST data set using learning rate $\eta = 10^{-3}$. The numbers above the bars correspond to the number of highly memorized observations in each bin. Randomly selected training observations from several bins are shown, with dashed lines illustrating the bin where the images in a particular column can be found. Images with a yellow frame are highly memorized whereas those with a blue frame have low memorization scores. Figure (b) shows the *proportion* of highly memorized and regular observations for each bin.

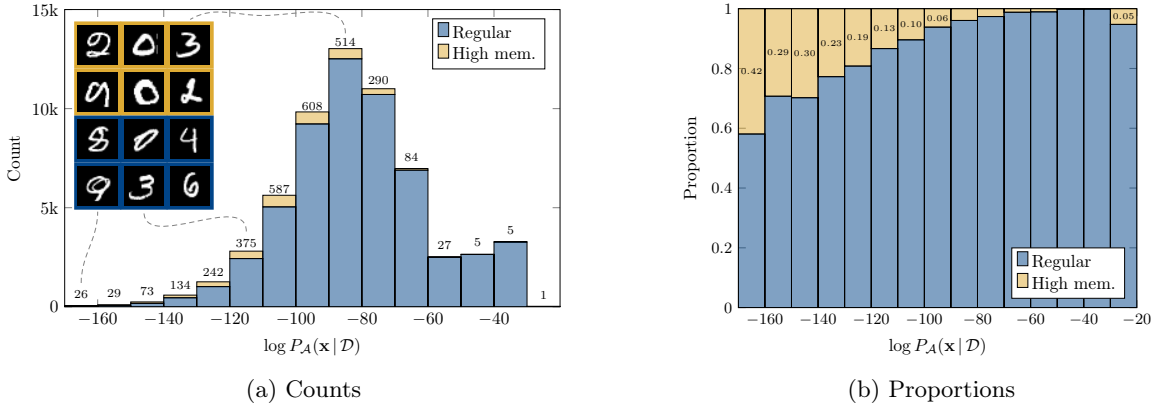


Figure 11: Similar to Figure 10, but for the VAE trained on MNIST with learning rate $\eta = 10^{-4}$.

C.3 Nearest Neighbors

The nearest neighbor experiments demonstrated in Section 4.4 are repeated below in Figures 12 and 13 for the VAEs trained on the MNIST data set using learning rates of 10^{-3} and 10^{-4} . For these models and data set we again do not see a clear relation between the nearest neighbor distance ratio ρ_i and the proposed memorization score M_i , as discussed in the main text.

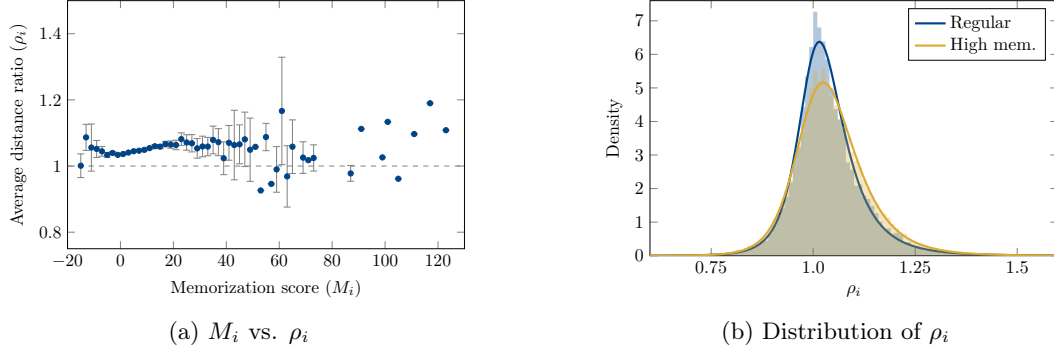


Figure 12: Illustration of the nearest neighbor distance ratio in (7) compared to the memorization score for a VAE trained on MNIST using a learning rate of $\eta = 10^{-3}$. We present the average of ρ_i for bins of the memorization score of width 2, and show error bars representing the confidence interval of the standard error of the mean of distance ratio measurements in each bin. The horizontal axis in figure (a) trims off one observation at $M_i \approx 210$ for clarity. Figure (b) shows the distribution of the distance ratio for observations with a high memorization score (top 5%) and the regular ones.

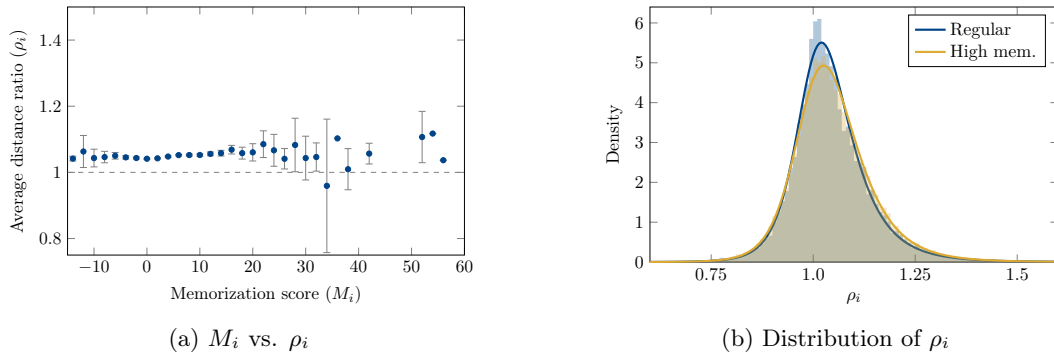


Figure 13: Similar to Figure 12 but for the VAE trained on MNIST using a learning rate of $\eta = 10^{-4}$. The horizontal axis in figure (a) trims off one observation at $M_i \approx 80$ for clarity.